

Fe₃O₄ nanosphere@multiporous organic networks: enhanced anode performances in lithium ion batteries through carbonization†

Cite this: *Chem. Commun.*, 2014, 50, 7723Received 19th March 2014,
Accepted 27th May 2014

DOI: 10.1039/c4cc02068e

www.rsc.org/chemcomm

Byungho Lim,^a Jaewon Jin,^a Jin Yoo,^a Seung Yong Han,^a Kyeongyeol Kim,^a Sungah Kang,^a Nojin Park,^a Sang Moon Lee,^a Hae Jin Kim^b and Seung Uk Son^{*a}

Very thin microporous organic networks were formed on the surface of Fe₃O₄ nanospheres by Sonogashira coupling of tetra(4-ethynylphenyl)methane and 1,4-diiodobenzene. The thickness was controlled by screening the number of building blocks. Through carbonization, Fe₃O₄@C composites were prepared. The Fe₃O₄@C composites with 4–6 nm carbon thickness showed promising reversible discharge capacities of up to 807 mA h g⁻¹ and enhanced electrochemical stability.

Recently, microporous organic network (MON) materials have been actively studied.¹ The covalent networking of rigid building blocks induces the microporosity in MONs. Based on the porosity and robustness of the MON materials, their application fields, including selective adsorption² and catalysis,³ are expanding. For a recent example, the heat-treatment of MON under an inert atmosphere resulted in the formation of porous carbon materials which have been further applied as charge storage materials for super-capacitor applications.⁴

Presently, lithium ion batteries (LIBs) are quite attractive energy storage devices.⁵ To improve storage capacity and operation stability, new electrode materials have to be designed and prepared continuously.⁶ In addition to the group IVA element-based materials such as Si or Sn nanomaterials, various metal oxides have been studied recently as anode materials.^{5,6} It has been documented that the metal oxides show promising storage capacities through a conversion mechanism to form zerovalent metal and lithium oxide.^{5,6} However, their low conductivity and capacity fading during operation are significant drawbacks. To enhance anode performances, metal oxide-carbon composites⁷ have been suggested

and prepared through the incorporation of metal oxides into carbon materials including graphene.^{7c} However, the homogeneous carbon coating on the metal oxides^{7d} may be a more straightforward method to enhance the conductivity and electrochemical stability. In this case, the porosity and tailored thickness control of the coating are important parameters.

The application of MON chemistry to energy storage devices has been relatively less explored.^{4,8} Our research group has studied the synthesis of functional MONs⁹ based on the Sonogashira coupling reaction¹⁰ and various inorganic electrode materials.¹¹ We reasoned that the microporous organic networking can be applied for the purpose of coating metal oxide anode materials through successive carbonization. Recently, our group has reported that silica spheres can be coated with MONs.¹² In this work, we report MON coated iron oxides, successive carbonization of iron oxide-carbon materials, and their electrochemical performances as anode materials in LIBs.

Fig. 1 shows the application of MON chemistry for the synthesis of porous carbon-coated iron oxide anode materials.

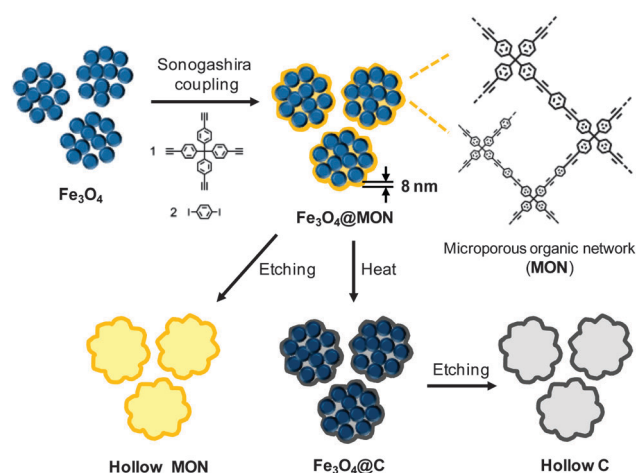


Fig. 1 Synthetic scheme for Fe₃O₄@MON, Fe₃O₄@C, hollow MON and hollow carbon materials.

^a Department of Chemistry and Department of Energy Science, Sungkyunkwan University, Suwon 440-746, Korea. E-mail: sson@skku.edu; Fax: +82-031-290-4572

^b Korea Basic Science Institute, Daejeon 350-333, Korea

† Electronic supplementary information (ESI) available: Experimental details; ¹³C NMR, PXRD, and the TGA curve of hollow MON; discharge capacities of Fe₃O₄@C-700 obtained through calcination of Fe₃O₄@MON-25; SEM and TEM images of Fe₃O₄@C-700 after 50 cycles; and EDS mapping images, pore-size distribution, cyclovoltammogram, charge-discharge curves and rate capabilities of Fe₃O₄@C-700. See DOI: 10.1039/c4cc02068e

First, nanoparticulate Fe_3O_4 spheres were prepared by a synthetic method in the literature.¹³ Through Sonogashira coupling reaction using 1 equiv. of tetra(4-ethynylphenyl)methane and 2 equiv. of 1,4-diiodobenzene,¹⁰ the Fe_3O_4 nanospheres were directly coated with MON (refer to the ESI† for the detailed procedure). The black color of the original Fe_3O_4 nanospheres changed to dark yellow. The resultant Fe_3O_4 @MON materials were systematically heated in the range of 600–800 °C under argon.

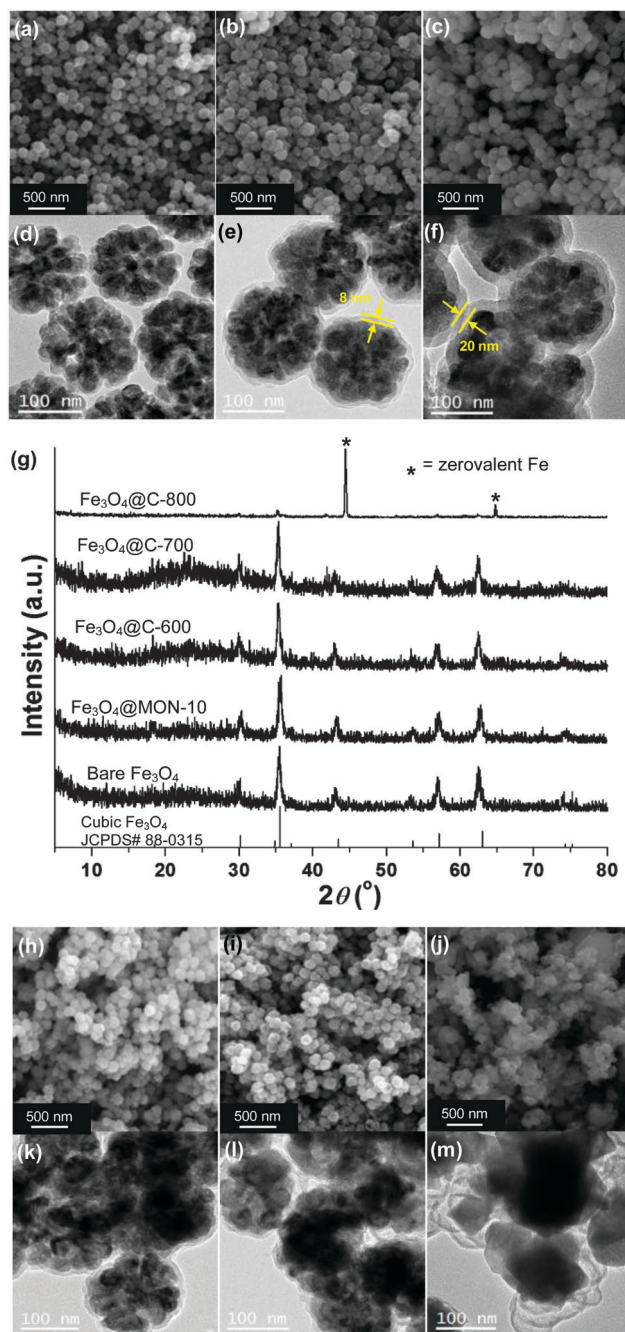


Fig. 2 SEM and TEM images of bare Fe_3O_4 (a, d), Fe_3O_4 @MON-10 (b, e) Fe_3O_4 @MON-25 (c, f), Fe_3O_4 @C-600 (h, k), Fe_3O_4 @C-700 (i, l), and Fe_3O_4 @C-800 (j, m); (g) PXRD patterns of bare Fe_3O_4 , Fe_3O_4 @MON-10, and Fe_3O_4 @C-600, 700, 800.

After heat-treatment, the materials became black through carbonization of MON on the Fe_3O_4 surface.

According to scanning (SEM) and transmission electron microscopy (TEM) studies, 140 nm-sized bare Fe_3O_4 nanospheres consist of 25 nm-sized small nanoparticles (Fig. 2a and d). The surface investigation of bare Fe_3O_4 nanospheres by TEM showed no sign of organic materials. In comparison, Fe_3O_4 @MON (denoted as Fe_3O_4 @MON-10) prepared using 10 mg of tetra(4-ethynylphenyl)methane showed a homogeneous and very thin MON coating on the surface of the Fe_3O_4 nanospheres (Fig. 2b and e). The thickness of the MON coating was measured to be 8–10 nm. When the amount of tetra(4-ethynylphenyl)methane increased to 25 mg, a MON thickness of ~20 nm in Fe_3O_4 @MON (denoted as Fe_3O_4 @MON-25) was observed (Fig. 2c and f).

According to powder X-ray diffraction (PXRD) studies, the original cubic phase of Fe_3O_4 was maintained after MON coating and even after calcination at 600 °C and 700 °C (Fig. 2g). The Fe_3O_4 @C materials obtained by heating Fe_3O_4 @MON-10 at 600 °C, 700 °C and 800 °C are denoted as Fe_3O_4 @C-600, Fe_3O_4 @C-700, and Fe_3O_4 @C-800, respectively. As shown in Fig. 2h and k, and in Fig. 2i and l, very thin carbon coatings in Fe_3O_4 @C-600 and Fe_3O_4 @C-700 were, respectively, observed. Their thicknesses were reduced from 8–10 nm (MON coating) to 4–6 nm through carbonization.¹⁴ In the case of Fe_3O_4 @C-800, the original inner iron oxides changed to angular shaped zerovalent Fe materials through reduction by carbon (Fig. 2j and m).

To characterize the MON and carbon coating in Fe_3O_4 @MON-10 and Fe_3O_4 @C-700, the inner Fe_3O_4 was etched by reaction with HCl. According to the TEM images, a homogeneous coating of MON and carbon materials could be confirmed (Fig. 3a and b). The shape of the inner empty space of hollow materials matched well with those of the original Fe_3O_4 nanospheres. According to N_2 sorption isotherm analysis, hollow MON and hollow carbon materials showed high surface areas of 406 $\text{m}^2 \text{g}^{-1}$ and 1093 $\text{m}^2 \text{g}^{-1}$, respectively. Interestingly, both materials showed not only microporosity of

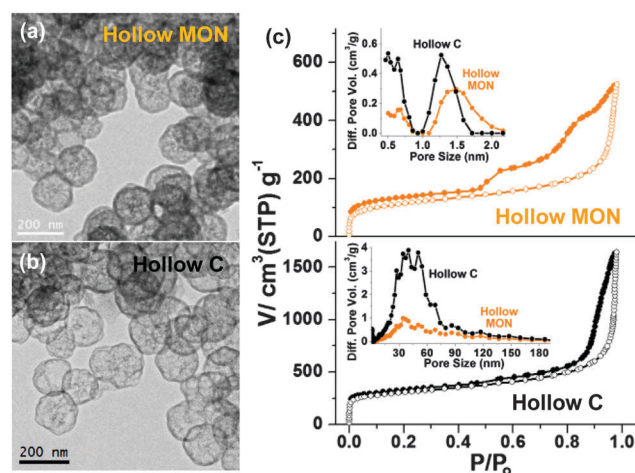


Fig. 3 TEM images of hollow MON (a) and hollow carbon materials (b) obtained from Fe_3O_4 @MON-10 and Fe_3O_4 @C-700, respectively, through chemical etching of Fe_3O_4 . (c) Their N_2 adsorption-desorption isotherm curves at 77 K and pore size distribution diagrams (inset of Fig. 3c, the DFT method was used for measurement of pore size distribution).

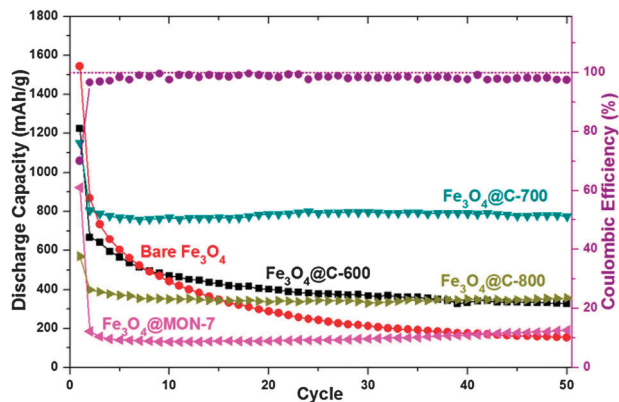


Fig. 4 Cycling performance of bare- Fe_3O_4 , Fe_3O_4 @MON-10, Fe_3O_4 @C-600–800, and coulombic efficiencies of Fe_3O_4 @C-700.

networks but also mesoporosity which originated from the etched iron oxide (Fig. 3c and inset).¹⁵ The solid phase ^{13}C nuclear magnetic resonance (NMR) spectroscopy confirmed the expected chemical components of two building blocks in MON (Fig. S1 in the ESI†). PXRD showed a typical amorphous character of hollow MON and hollow carbon (Fig. S2 in the ESI†). Thermogravimetric analysis showed that the MON starts to decompose at 210 °C under N_2 (Fig. S3 in the ESI†).

Considering the homogeneous carbon coating in Fe_3O_4 @C materials, their electrochemical performance as anode materials in LIB was studied (refer to the ESI† for the detailed procedure). Fig. 4 summarizes the results with a current density of 50 mA g^{-1} .

The bare Fe_3O_4 nanospheres showed a discharge capacity of 869 mA h g^{-1} in the 2nd cycle which was sharply decreased to 153 mA h g^{-1} in the 50th cycle (only 18% retention of the 2nd capacity). The Fe_3O_4 @MON-10 showed a very poor discharge capacity of 185 mA h g^{-1} in the 2nd cycle due to the insulating effect of the MON coating. Fe_3O_4 @C-600 showed a 49% capacity retention in the 50th run, compared with a capacity of 667 mA h g^{-1} in the 2nd cycle. Fe_3O_4 @C-700 showed the best performance with 806 mA h g^{-1} and 775 mA h g^{-1} (96% capacity retention) discharge capacities in the 2nd and 50th cycle, respectively.¹⁶ Fe_3O_4 @C-800 showed a discharge capacity of 399 mA h g^{-1} in the 2nd cycle due to the phase change of iron oxide. When the thickness of the carbon coating increased from 4–6 nm to 15 nm, the discharge capacity of Fe_3O_4 @C (calcination of Fe_3O_4 @MON-25 at 700 °C) decreased to 628 mA h g^{-1} in the 2nd cycle, due to the increased carbon contents (Fig. S4 in the ESI†).¹⁴

The theoretical anode capacities of Fe_3O_4 and graphite are known to be 924 mA h g^{-1} (ref. 7) and 372 mA h g^{-1} (ref. 6) respectively. Thus, considering the 11 wt% carbon contents,¹⁷ the reversible capacity (806 mA h g^{-1}) of Fe_3O_4 @C-700 corresponds to 93% of the theoretical maximum value. The recovered Fe_3O_4 @C-700 after 50 cycles maintained the composite structure (Fig. S5 in the ESI†). The coulombic efficiency of Fe_3O_4 @C-700 was 70% in the 1st cycle, rapidly reaching 97% in the 2nd cycle, and was maintained above 97% in successive cycles (Fig. 4). The discharge voltage profile of Fe_3O_4 @C-700 showed a plateau at 0.8 V (vs. Li/Li^+) in the 1st cycle and shoulder peaks at 1.0 V in the 2nd–50th cycles, which concurs

with the known behavior of the Fe_3O_4 anode materials (Fig. S6 in the ESI†).⁷ The cyclic voltammogram confirmed that the observed electrochemical events are based on the conversion mechanism of iron oxides (Fig. S7 in the ESI†).^{7,18} Fe_3O_4 @C-700 showed a promising rate capability (Fig. S6 in the ESI†). When the current density increased to 100, 200, and 500 mA h g^{-1} , the discharge capacities of 760, 709, and 615 mA h g^{-1} , respectively, were observed. Even with a current density of 1.0 A g^{-1} , the cells maintained a capacity of 536 mA h g^{-1} , which is much higher than that of commercialized graphite (372 mA h g^{-1}).⁶ The performances of Fe_3O_4 @C-700 are superior or comparable to those (480–570 mA h g^{-1} capacities at a current density of 500 mA g^{-1}) of the Fe_3O_4 -carbon materials (21–44 w% carbon) prepared by using glucose or polymers as carbon sources.^{7d-f}

In conclusion, this work showed that MON chemistry can be successfully applied for the enhancement of electrochemical performances of electrode materials in LIBs through successive calcination. We believe that based on the synthetic strategy in this work, more diverse inorganic anode materials with very thin carbon coating can be prepared by screening various metal oxides.

This work was supported by grant NRF-2012-R1A1A2004029 (Basic Science Research Program) through the National Research Foundation of Korea funded by the MEST.

Notes and references

- Recent reviews on MONs: (a) R. Dawson, A. I. Cooper and D. J. Adams, *Prog. Polym. Sci.*, 2012, **37**, 530; (b) F. Vilela, K. Zhang and M. Antonietti, *Energy Environ. Sci.*, 2012, **5**, 7919; (c) A. Thomas, *Angew. Chem., Int. Ed.*, 2010, **49**, 8328.
- Selected examples: (a) X. Yang, B. Li, I. Majeed, L. Liang, X. Long and B. Tan, *Polym. Chem.*, 2013, **4**, 1425; (b) C. D. Wood, B. Tan, A. Trewin, F. Su, M. J. Rosseinsky, D. Bradshaw, Y. Sun, L. Zhou and A. I. Cooper, *Adv. Mater.*, 2008, **20**, 1916.
- Selected examples: (a) K. Thiel, R. Zehbe, J. Roeser, P. Strauch, S. Enthaler and A. Thomas, *Polym. Chem.*, 2013, **4**, 1848; (b) C. Bleschke, J. Schmidt, D. S. Kundu, S. Blechert and A. Thomas, *Adv. Synth. Catal.*, 2011, **353**, 3101; (c) X. Du, Y. Sun, B. Tan, Q. Teng, X. Yao, C. Su and W. Wang, *Chem. Commun.*, 2010, **46**, 970.
- Review: L. Hao, X. Li and L. Zhi, *Adv. Mater.*, 2013, **25**, 3899.
- P. Poizat, S. Laruelle, S. Grugeon, L. Dupont and J.-M. Tarascon, *Nature*, 2000, **407**, 496.
- Recent review: (a) H. B. Wu, J. S. Chen, H. H. Hng and X. W. Lou, *Nanoscale*, 2012, **4**, 2526; (b) L. Ji, Z. Lin, M. Alcoutlabi and X. Zhang, *Energy Environ. Sci.*, 2011, **4**, 2682.
- Recent examples: (a) C. He, S. Wu, N. Zhao, C. Shi, E. Liu and J. Li, *ACS Nano*, 2013, **7**, 4459; (b) M. Latorre-Sanchez, A. Primo and H. Garcia, *J. Mater. Chem.*, 2012, **22**, 21373; (c) G. Zhou, D.-W. Wang, F. Li, L. Zhang, N. Li, Z.-S. Wu, L. Wen, G. Q. Lu and H.-M. Cheng, *Chem. Mater.*, 2010, **22**, 5306; (d) W.-M. Zhang, X.-L. Wu, J.-S. Hu, Y.-G. Guo and L.-J. Wan, *Adv. Funct. Mater.*, 2008, **18**, 3941; (e) B. Jang, M. Park, O. B. Chae, S. Park, Y. Kim, S. M. Oh, Y. Piao and T. Hyeon, *J. Am. Chem. Soc.*, 2012, **134**, 15010; (f) T. Yoon, C. Chae, Y.-K. Sun, X. Zhao, H. H. Kung and J. K. Lee, *J. Mater. Chem.*, 2011, **21**, 17325.
- (a) N. Kang, J. H. Park, J. Choi, J. Jin, J. Chun, I. G. Jung, J. Jeong, J.-G. Park, S. M. Lee, H. J. Kim and S. U. Son, *Angew. Chem., Int. Ed.*, 2012, **51**, 6626; (b) H. S. Lee, J. Choi, J. Jin, J. Chun, S. M. Lee, H. J. Kim and S. U. Son, *Chem. Commun.*, 2012, **48**, 94.
- (a) N. Kang, J. H. Park, K. C. Ko, J. Chun, E. Kim, H. W. Shin, S. M. Lee, H. J. Kim, T. K. Ahn, J. Lee and S. U. Son, *Angew. Chem., Int. Ed.*, 2013, **52**, 6228; (b) J. Chun, J. H. Park, J. Kim, S. M. Lee, H. J. Kim and S. U. Son, *Chem. Commun.*, 2012, **24**, 3458; (c) J. Chun, J. H. Park, J. Kim, S. M. Lee, H. J. Kim and S. U. Son, *Chem. Mater.*,

- 2012, **24**, 3458; (d) H. C. Cho, H. S. Lee, J. Chun, S. M. Lee, H. J. Kim and S. U. Son, *Chem. Commun.*, 2011, **47**, 917.
- 10 J.-X. Jiang, F. Su, A. Trewin, C. D. Wood, N. L. Campbell, H. Niu, C. Dickinson, A. Y. Ganin, M. J. Rosseinsky, Y. Z. Khimyak and A. I. Cooper, *Angew. Chem., Int. Ed.*, 2007, **46**, 8574.
- 11 (a) J. Xu, J. Jin, K. Kim, Y. J. Shin, H. J. Kim and S. U. Son, *Chem. Commun.*, 2013, **49**, 5981; (b) J. Xu, K. Jang, J. Choi, J. Jin, J. H. Park, H. J. Kim, D.-H. Oh, J. R. Ahn and S. U. Son, *Chem. Commun.*, 2012, **48**, 6244; (c) J. Choi, J. Jin, I. G. Jung, J. M. Kim, H. J. Kim and S. U. Son, *Chem. Commun.*, 2011, **47**, 5241.
- 12 N. Kang, J. H. Park, M. Jin, N. Park, S. M. Lee, H. J. Kim, J. M. Kim and S. U. Son, *J. Am. Chem. Soc.*, 2013, **135**, 19115.
- 13 J. Ge and Y. Yin, *Adv. Mater.*, 2008, **20**, 3485.
- 14 For the EDS mapping of Fe₃O₄@C-700, see Fig. S8 in the ESI†.
- 15 For the porosity analysis of Fe₃O₄@C-700, see Fig. S9 in the ESI†.
- 16 For the extended cycling performance, see Fig. S10 in the ESI†.
- 17 Elemental analysis revealed 11 wt% and 16 wt% carbon contents in Fe₃O₄@C-700 obtained using Fe₃O₄@MON-10 and -25, respectively.
- 18 The corresponding electrochemical reaction is as follows: Fe₃O₄ + 8Li + 8e⁻ ↔ 3Fe + 4Li₂O.